# MODELING & DESIGNING OF A SOLAR FURNACE FOR CURING GEOPOLYMER BRICKS

## Mona A. Mahmoud[1], M. Helmy[2], M. Morsy [3] and A. Abd El-Al.[4&*]

[1] Grad. Stud., Ag. and Bio. Eng., Fac. of Ag., EL-Shatby, Alex. U., Egypt.

[2] Prof., Dr. of Bio-Environmental Sys. Eng. & Energy, Ag. and Bio. Eng., Fac. of Ag., EL-Shatby, Alex. U., Egypt.

[3] Assoc. Prof., Dr. of Bio-Environmental Sys. Eng., Ag. and Bio. Eng., Fac. of Ag., EL-Shatby, Alex. U.,Egypt.

[4] Assist. Prof., Dr. of irrigation Sys., Ag. and Bio. Eng., Fac. of Ag., EL-Shatby, Alex. U., Egypt.

* E-mail: donya_ahmeds@hotmail.com
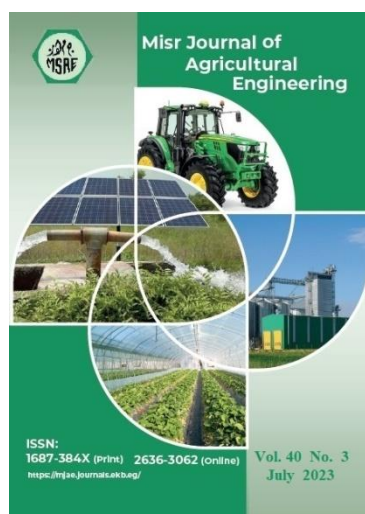
© Misr J. Ag. Eng. (MJAE)

**Keywords:**

Renewable energy; Computer models; Solar furnace; Friendly bricks.

## ABSTRACT

*This research was devoted to design an unfired brick solar furnace, heated and powered using solar energy. Mathematical model was developed to predict the configuration and performance of a system consisting of several components to produce geopolymer bricks. A computer program by using JavaScript consisting of a main routing and three subroutines was developed. The sizes of the solar collector and of solar panel are the performance of the interior heat exchangers. The temperature of the bricks was predicted. Error analysis techniques are used to validate the predicted results versus the measured values. The predicted results show good agreement with the measured values ($R^2 = 0.9823$). Also, the output results indicated directly the heating load required inside the solar furnace to dry the unfired brick with a designed interior air temperature at 100°C range between maximum heating load required "916.72 Watt" at midnight and the minimum value "810 Watt" at near noon. Output results of the computer models were used afterwards for design and construct the solar furnace system for curing unfired bricks.*

## 1. INTRODUCTION

The traditional manufacture in brick industry has showed a dramatic increase in energy consumption of fossil fuels nonrenewable which led to uneconomical process. High density polyethylene conventional red clay brick made of clay, sand, plastic and non-plastic components are burned in kilns with temperatures between 900 and 1100 °C, **(Chang, Hong, and Lin, 2016)**.

The dramatic increase in oil prices and expected shortages and Interruptions in the near future have become major concern to most industries especially with those which have intensive uses of energy such as the brick industry, **(Shakir and Mohammed, 2013)**.

From the eco-environmental point of view, the conventional methods of brick making have also caused serious environmental contamination represented by the enormous emission of

greenhouse gases. They resulted in unusual climate changes causing smog, acid rains, and global warming.

So, the use of fossil fuels is responsible for economic, energy, environmental problems, and ecological issues. The red brick industry suffers from rising prices of energy plus other related environmental problems such as carbon dioxide, fluorine, and sulfur emission, **(Bhat et al., 2014)**. Firing red clay or cement bricks should be prohibited or at least to be reduced to minimum from the manufacturing process. The brick industry in the future should be held in an ecological basic, **(Sudharsan and Palanisamy, 2018)**. Few studies have been conducted in developing bricks in an eco-environmental method.

To eliminate the environmental problems evolved from red brick traditional manufacturing materials other materials than the traditional materials (cement, clay, etc.) have been sought by several researchers. Geopolymers have been found to have many useful characteristics and benefits for brick industry and to be most appropriates alternative solution for brick industry.

Geopolymers are environmentally friendly. They don't emit greenhouse gases during polymerization process. They also require less energy for brick manufacturing process **(Turner and Collins, 2013)**. Geopolymer technology is more economical since it makes use of marginal material such as flay ash and slag **(Kayali, Khan, and Ahmed, 2012)**. It also uses less energy.

One of the very important characteristics of the geopolymer as an alternative material is the low temperature required for curing the bricks (around 70: 90 ˚C). This low temperature makes it possible and economical to use solar energy as a source of energy for curing bricks.

Thus, the aim of this work is to seek the use of cheap, clean, and sustainable source of energy which reduces environmental pollution resulting from the use of other energy sources, and to produce environmentally friendly bricks under Egyptian conditions and by treating the industrial wastes.

More specific objectives are:

1. To examine the possibility of using solar energy for thermal treatment and powering an unfired brick solar furnace system which produces, an environmentally friendly and energy sustainable for brick Industry.

2. To develop a mathematical model and a computer simulation program to design an optimum performing, solar heated and powered unfired brick furnace system.

3. To determine optimal configuration of the design parameters for sizing the system based on the verified results of the simulation program.

## 2. MATERIALS AND METHODS

**SYSTEM DESCRIPTION**

A schematic diagram is shown in Figure (1). The primary components of the solar furnace are:

1. A high temperature solar collector consisting of fixed concentrator with evacuated tubular absorber.

2. A passive downward heat transfer system to transfer energy from the solar collector to the energy storage.

3. A thermal energy storage unit with conventional energy backup during the night.

4. A thermal energy transfer system between the thermal energy store and the solar furnace.

5. A heat exchanger tubes set up installed on all internal surface of walls of the solar furnace to heat up the interior furnace microclimate by radiation and convection (from tube of heat exchanger) both at the same time in parallel.

6. Solar panel to generate the electricity needed. For instance, operating the pump and the temperature control system as well as storing solar energy inside the battery for use at night.

7. The external solar collector. The system was automatically controlled by a control system. It operated and powered entirely by a solar energy provided by an external solar collector. The control system included temperature control cards, battery, invertor, and charger. A closed circuit consisted of the solar collector, control system, a liquid circulation pump delivered the fluid throughout the cycle, and a thermostat. It was used to sense and measure interior air temperature. When the solar furnace interior air temperature reached the designed and designed temperature, the control system disconnects the circuit and the pump will automatically shut down. Accordingly, the whole system became environmentally friendly

## MODEL DEVELOPMENT

In order to examine test, the possibility of using an unfired brick solar furnace to provide a clean, cheap, and sustainable energy source for brick industry, optimal configurations of the design parameters for sizing the system were first mathematically simulation before the construction and field tests. Mathematical modeling and simulation computer programs were developed to carry out the analysis for the selection of an optimum system design. A computer Software written in JavaScript was used.

The solar furnace system consists of the following main components:

1. Unfired brick solar furnace.
2. A heat exchanger interior furnace heat exchanger, Figure (2).
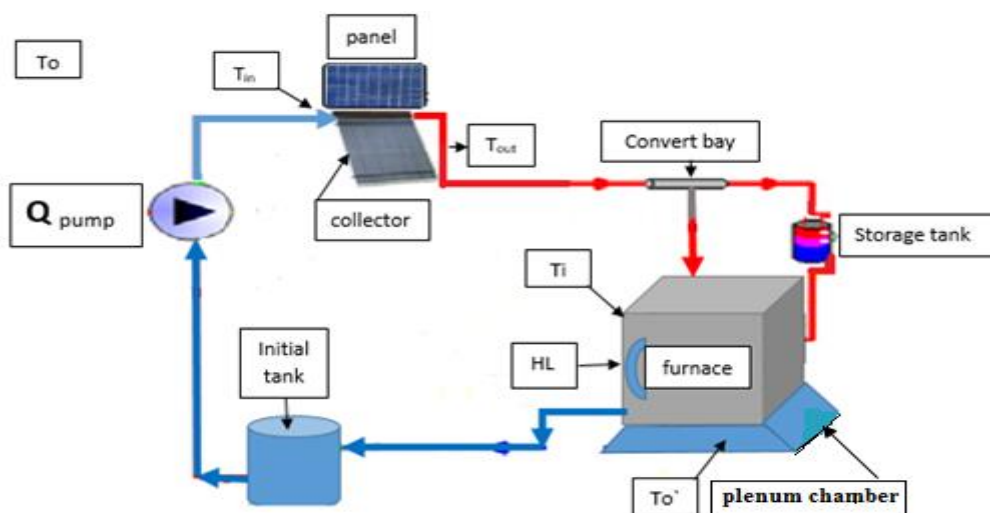3. Vacuum tubes solar collector.



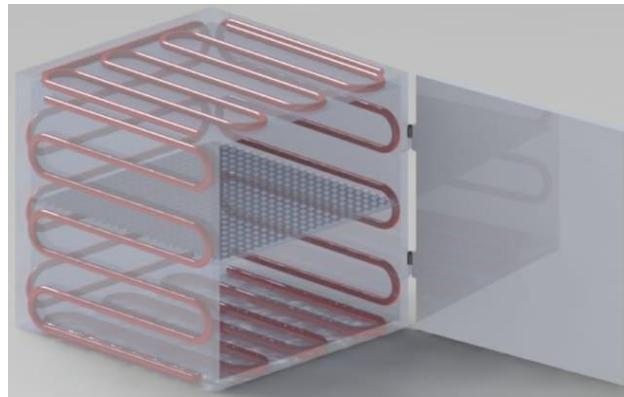**Figure (1): The main thermal system components**

**Figure (2): A heat exchanger around the solar furnace**

4. A thermal storage tank.
5. Solar panel.

A main program and three subprograms were developed to carry out the system analysis to design and describe the performance of an unfired brick solar furnace system. The main program was developed to determine the furnace heating load required to dry the unfired brick. One subprogram was developed to predict the brick temperature; the second subprogram was to predict the surface ground temperature $T_g$ beneath the furnace using the finite difference technique; and the last subprogram was developed to predict the air temperature in the plenum chamber beneath the solar furnace.

**Unfired brick solar furnace mathematical simulation model**

The design for the modification and control unfired brick solar furnace required an accurate prediction of the heating load required to dry bricks at a predetermined temperature above the ambient between 70 ˚C & 90 ˚C was carried out at one hour time interval for 24 hours based upon physical and environmental factors. Such factors are the solar furnace configuration and material, ambient air temperatures, and interior natural air movement. The ambient temperatures were fed into the model as input data for 24 hours per day. The following energy balance equation was used to determine the heating load required for the solar furnace to dry the geopolymer bricks. It was developed based upon the energy analysis of the solar furnace microclimate.

$$HL = D_c + D_w + D_f + R_{f\text{-}b} + R_{w\text{-}b} + R_{c\text{-}b} + C_{a\text{-}b} + V, \ J/s \dots\dots\dots\dots\dots \textbf{(1)}$$

$$D_C = U_c \ A_c \ (T_i - T_o), \ J/s \dots\dots\dots\dots\dots \textbf{(2)}$$

$$D_W = U_w \ A_w \ (T_i - T_o), J/s \dots\dots\dots\dots\dots \textbf{(3)}$$

$$D_f = U_f * A_f * \ (T_i - T_o'), J/s \dots\dots\dots\dots\dots \textbf{(4)}$$

$$C_{a-b} = h * A_b * (T_i - T_b), J/s \dots\dots\dots\dots\dots \textbf{(5)}$$

$$V = = \vartheta * A * (h_i - h_r) * \rho_r * D_t * N, J/s \dots\dots\dots\dots\dots \textbf{(6)}$$

Where:

$\vartheta$: average velocity m/s the typical air velocity through a door assumed from 0.3 to 1.5 m/s, (**ASHRAE Handbook 2001**).

A: area of opening door m² the leakage area can vary from 0.03 m2 to over 0.1 m2 per door, (ASHRAE Handbook 2001). The various components affecting heat load computations are shown in Figure (3). Bricks were assumed to be placed on a perforated plate fixed to the walls installed inside the furnace.
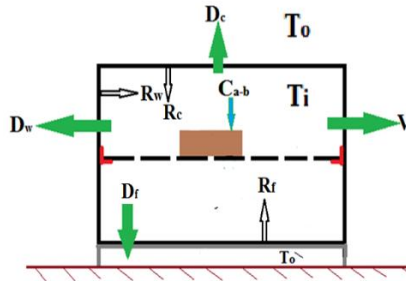


**Figure (3): A schematic diagram of energy analysis in a brick furnace**

## Brick energy balance simulation model

The simplest method for predicting brick temperature inside the solar furnace was carried out by performing an energy balance on the brick. In this method, the developed simulation computer program depended upon five major components that affected the brick temperature. The following equation was developed to carry out this energy analysis.

$$R_{f\text{-}b} + R_{w\text{-}b} + R_{c\text{-}b} + C_{a\text{-}b} + D_{p\text{-}b} = m_b\,(Cp_b)\left(\frac{Tb^+ - Tb}{\Delta\tau}\right) \quad\dots\dots\dots\dots\dots\dots\dots\dots\text{(7)}$$

$$R_{f\text{-}b} = \varepsilon_f \varepsilon_b\,(A_f)(F_{(f-b)})(\sigma)\left(T_f^4 - T_b^4\right), \text{J/s} \quad\dots\dots\dots\dots\dots\dots\text{(8)}$$

$$R_{w\text{-}b} = \varepsilon_w \varepsilon_b\,(A_w)(F_{(w-b)})(\sigma)\left(T_w^4 - T_b^4\right), \text{J/s} \quad\dots\dots\dots\dots\dots\text{(9)}$$

$$R_{c\text{-}b} = \varepsilon_c \varepsilon_b\,(A_c)\,(F_{(c-b)})(\sigma)\left(T_c^4 - T_b^4\right), \text{J/s} \quad\dots\dots\dots\dots\dots\text{(10)}$$

$$D_{P-b} = U_p\,A_{p-b}\left(T_i - T_b\right), \text{J/s} \quad\dots\dots\dots\dots\dots\dots\dots\dots\text{(11)}$$

where:

$$U_p = \frac{1}{\frac{\Delta X_p}{K_p} + \frac{1}{h_i}}\,, \frac{w}{m^2.c^\circ} \quad\dots\dots\dots\dots\dots\dots\dots\dots\text{(12)}$$

h = The convection heat transfer coefficient = (Nu*k)/L , W/m² K ……………… **(13)**

Nu is the Nusselt number = C•(Ra)$^n$ ……………………………………………… **(14)**

C and n are constants and their values from tables

Ra = the Raleigh number = Gr′•Pr ………………………………...………………. **(15)**

The shape factors $F_{(f\text{-}b)}$, $F_{(w\text{-}b)}$, and $F_{(c\text{-}b)}$, were assumed $F_{f\text{-}b} = F_{w\text{-}b} = F_{c\text{-}b} = 1$

It is important to say that, the initial temperature of the brick, $T_b$, at the starting of running the computer simulation model was assumed equal to the ambient temperature $T_o$. This was done since the brick was placed on the ambient conditions for more than twenty four hours curing time. The main factors affecting brick temperature are indicated in Figure (4).
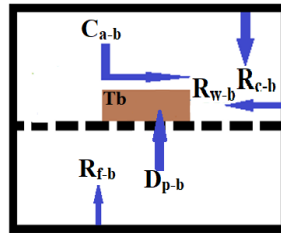
**Figure (4): Factors affecting brick temperature**

Furnace floor temperature $T_f$, was determined as follows:

**Ground surface temperature simulation model**

To determine the surface ground temperature $T_g$, using a numerical method. A computer subprogram was developed.

$$\frac{\partial^2 T}{\partial x^2} + \frac{\partial^2 T}{\partial y^2} + \frac{\partial^2 T}{\partial z^2} + \frac{G}{k} = \frac{1}{\alpha}\left[\frac{\partial T}{dt}\right] \quad\text{.............................................................. (16)}$$

Equation (16) was used to describe the transient temperature distribution in a solid slab. To solve this equation numerically, finite-difference technique was used. The advantage of the explicit forward-difference procedure is the direct calculation of the future nodal temperature. In other words, the nodal temperature at advanced time increment was expressed in terms of the surrounding nodal temperature at the beginning of the time increment. Accordingly, the calculation of the nodal temperature directly proceeded from one-time increment to the next until the temperature distribution was calculated at the desired final state. However the stability of this procedure was governed by the selection of the increment of ground depth $\Delta z$ and increment of time $\Delta\tau$ values since the small chosen value of $\Delta z$ automatically forced the selection of $\Delta\tau$ to the maximum.

**Model assumptions:**

1- An infinite layer of the ground of thickness $\Delta z$ in Z direction.
2- One dimensional heat flow in the Z direction.
3- The ground thickness was divided into elements (nodes) as shown in Figure (5).
4- No external heat generation.
5- The ground thermal properties were depth Independent and held constant through the
6- Depth chosen.
7- The ground surface was principally subjected to uniform conditions of convection.
8- No solar radiation was available at the ground surface beneath the solar furnace.
9- The initial and boundary conditions were:

$$\text{at } \tau = 0, T_g = T_\infty \text{ (mean temp.)} \qquad \text{for Z.}$$

$$\text{at Z} = 0, -k_g\frac{\partial T_g}{\partial z} = h_g(T_o - T_g) + \gamma(I) - E \qquad \text{for all } \tau > 0.0 \quad\text{................... (17)}$$

$$\text{at Z} = \delta, T_g = T_\infty \qquad \text{for all } \tau > 0.0 \text{ \& for } \delta \to \infty$$

The prediction of temperature for an interior node was calculated using equation (16) for the interior nodes (Holman, 1981). Equation (18) was modified to predict the temperature at the surface node. The modification was carried out to include the possibility of temperatures variation due to solar radiation and evaporation. The nomenclature for an interior and a surface node subjected to various conditions are shown in Figure (5).

$$T_m^{p+1} = \frac{\alpha\,\Delta\tau}{\Delta Z^2}\left[2\frac{h\,\Delta Z}{k}\,T_\infty + 2\,T_{m-1}^p + (1-E)\left[2\frac{\gamma(I)\Delta Z}{k}\right] + \left[\frac{\Delta Z^2}{\alpha\,\Delta\tau} - 2\frac{h\,\Delta Z}{k} - 2\right]T_m^p\right] \quad\text{......................... (18)}$$

for stability conditions of equations (18), the Fourier number ($F_o = \frac{\alpha\,\Delta\tau}{\Delta Z^2}$) for the interior nodes for one dimensional system must be less or equal to 0.5, (Holman, 1981).
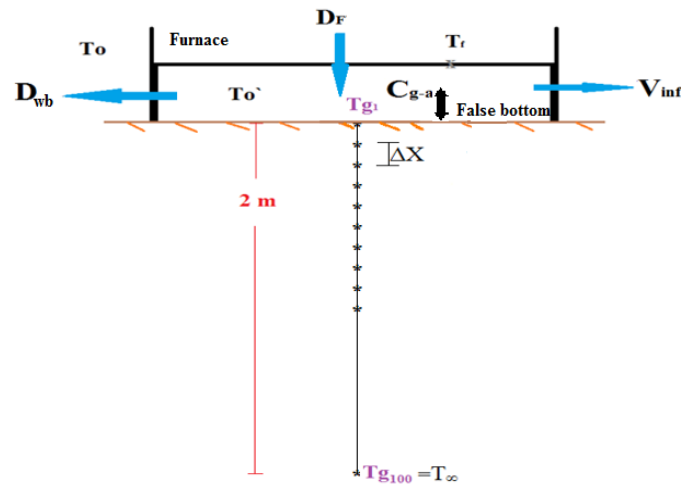
**Plenum air chamber temperature simulation model:**



**Figure (5): The factors affecting plenum chamber air temperature; $T_o$`**

An energy balance was applied on the microclimate space under the furnace as shown in Figure (5). The balance equation can be written as follow:

$$D_{f-p} \pm C_{g-a} - D_{Wb} + V_{inf} = 0.0 \quad\text{..............................................................(19)}$$

$$D_{Wp} = U_{wp} A_{wp} (T_O^` - T_O) \quad\text{.....................................................(20)}$$

The plenum chamber air temperature, $T_O^`$, is determined using computer subprogram.

The computational steps used in the mathematical simulation model are summarized as follows:

1- Input data and steps:
   a. Ambient air temperatures for 24 hours.
   b. Physical and thermal specifications including convective and over all heat transfer coefficients.
2- First subprogram to predict, $T_g$.
3- The second subprogram to predict, $T_o$`.
4- The third subprogram to predict, $T_b$.
5- The main program to predict HL.

A flow chart of the computer program is shown in Figures (6 & 7).

**System Components**

**1- Collector vacuum tubes**

An evacuated tubular solar collector was selected to supply the high temperature required (100 ˚C) for the furnace interior environment. The evacuated tube collector consists of a number of rows of parallel transparent glass tubes connected to a thermal radiation header pipe. These glass tubes are cylindrical in shape which means the angle of sunlight is always perpendicular to the heat absorption tubes. Evacuated tube collector is quite often made up of a single or multiple rows of parallel transparent glass tubes supported on a frame. The angle of collector slope was at $30^0$ as recommended by (**Jamal, Tangkemanda and Susanto., 2018**). Each tube consists of a "twin-glass tube" thick glass outer tube and a thinner glass inner tube. It was covered with a special coating that absorbs solar energy but eliminate heat loss. The tubes are made of borosilicate or soda lime glass which is strong, resistance to high temperatures, and has a high transmittance for solar radiation.
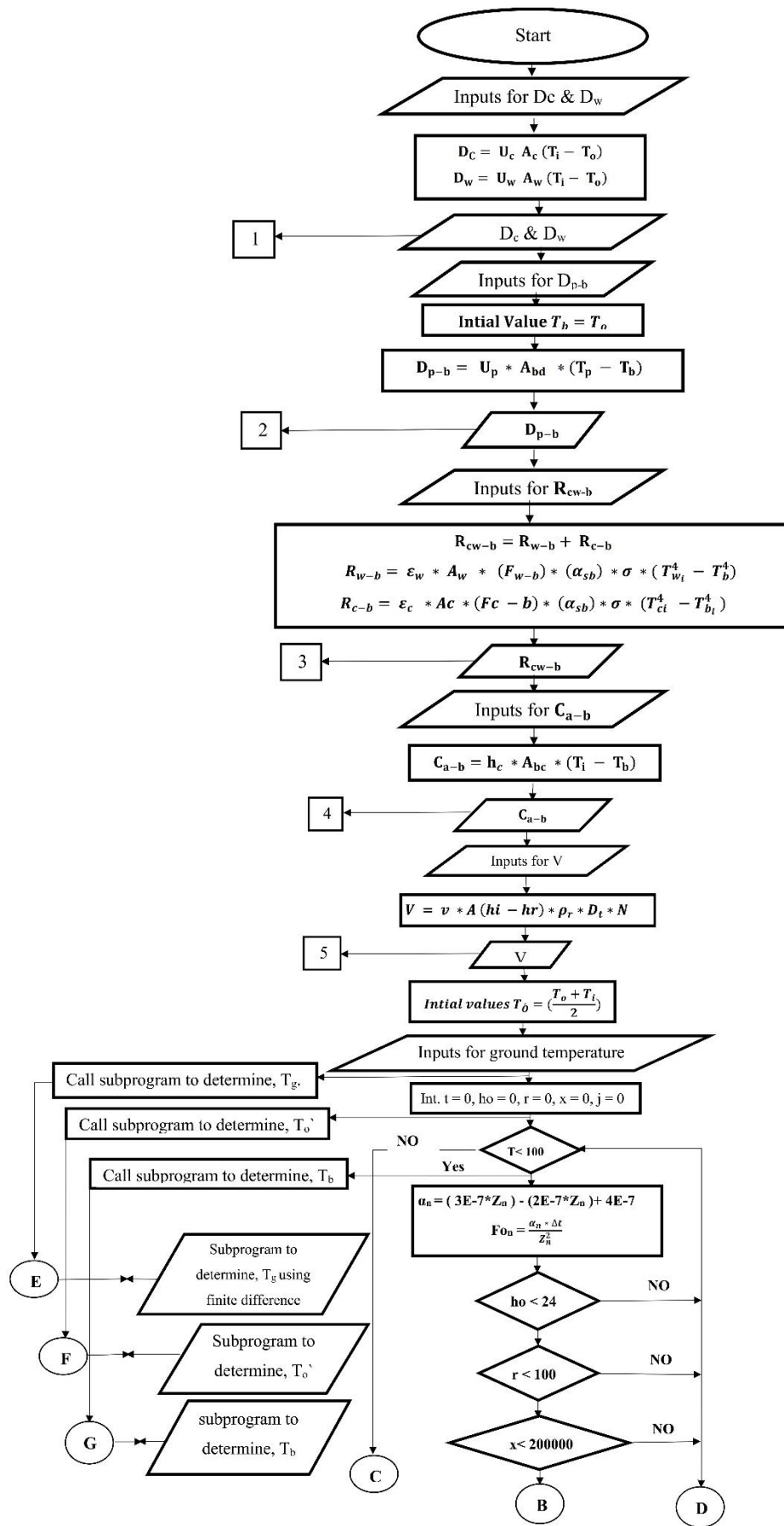
Start

Inputs for Dc & Dw

$$D_C = U_c \, A_c \, (T_i - T_o)$$
$$D_w = U_w \, A_w \, (T_i - T_o)$$

1 ← $D_c$ & $D_w$

Inputs for $D_{p-b}$

**Intial Value** $T_b = T_o$

$$D_{p-b} = U_p * A_{bd} * (T_p - T_b)$$

2 ← $D_{p-b}$

Inputs for $R_{cw-b}$

$$R_{cw-b} = R_{w-b} + R_{c-b}$$
$$R_{w-b} = \varepsilon_w * A_w * (F_{w-b}) * (\alpha_{sb}) * \sigma * (T_{w_i}^4 - T_b^4)$$
$$R_{c-b} = \varepsilon_c * Ac * (Fc - b) * (\alpha_{sb}) * \sigma * (T_{ci}^4 - T_{b_i}^4)$$

3 ← $R_{cw-b}$

Inputs for $C_{a-b}$

$$C_{a-b} = h_c * A_{bc} * (T_i - T_b)$$

4 ← $C_{a-b}$

Inputs for V

$$V = v * A \, (hi - hr) * \rho_r * D_t * N$$

5 ← V

$$Intial\ values\ T_{\dot{0}} = (\frac{T_o + T_i}{2})$$

Inputs for ground temperature

Call subprogram to determine, $T_g$.

Int. t = 0, ho = 0, r = 0, x = 0, j = 0

Call subprogram to determine, $T_o$'

NO

Call subprogram to determine, $T_b$

T< 100

Yes

$$\alpha_n = (\,3E\text{-}7*Z_n\,) - (2E\text{-}7*Z_n) + 4E\text{-}7$$
$$Fo_n = \frac{\alpha_n * \Delta t}{Z_n^2}$$

E ← Subprogram to determine, $T_g$ using finite difference

ho < 24 → NO

F ← Subprogram to determine, $T_o$'

r < 100 → NO

G ← subprogram to determine, $T_b$

x< 200000 → NO

C

B          D

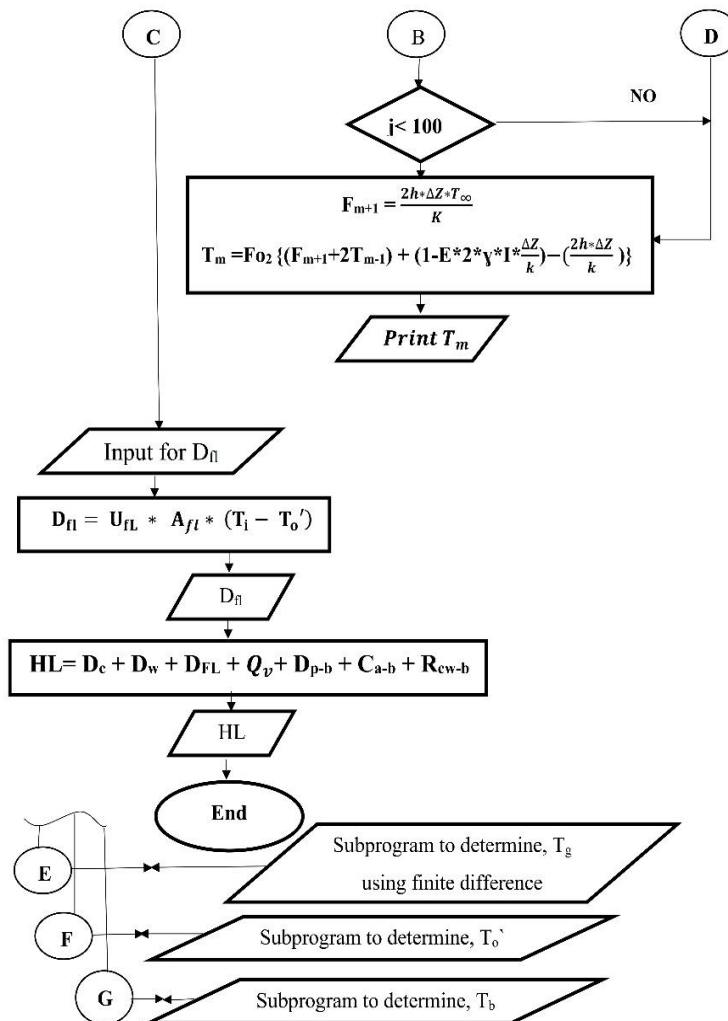**Figure (6): Flow chart to calculate heating load (continue)**

**Figure (7): Flow chart to calculate heating load**

Evacuated tube collectors do not heat the water directly in the tubes. Instead, air is removed or evacuated from the space between the two tubes, forming a vacuum, hence the name is evacuated tubes. This vacuum acts as an insulator reducing any significant heat loss to the surrounding atmosphere. It makes this type of collectors much more efficient than the flat plate types. Inside each glass tube, a flat or curved copper fin is attached to a metal heat pipe running through the inner tube. The fin is covered with a selective coating that transfers heat to the fluid circulating through the pipe. This sealed copper pipe transfers the solar heat to the header tank. The copper pipes are all connected to a common manifold which is then connected to the storage tank.

**2- Solar furnace heat exchanger**

In order to select the heat exchanger tubes installed inside the solar furnace to provide the heating load required to keep the interior furnace air temperature at the desired level, the output results of the heating loads from the mathematical simulation model were used to determine the tubes number and size. The selection included the length, diameter, number of spiral pipes, and pitch between spiral pipes. It was taken into account that the installation of the heat exchanger will cover the four walls of the solar furnace.

**3- Thermal storage tank**

Thermal energy storage is a technology that stocks thermal energy by heating a storage medium so that stored energy which can be used at later time for heating applications

**(Shawabkeh, 2015)**. This technology provides a way for reducing the energy demand and costs of operation. It consists of two cylinders made of stainless steel inside each other. There was a heat insulator from fiber glass between them to keep the heat and doesn't allow any heat losses. The inner cylinder has a heat exchanger made of copper in the form of a circular spring. The storage tank has two entrance one for the entry of the hot water from manifold to the heat exchanger and the other to enter the liquid that retains heat around the heat exchanger. It has also two outlets, one for exit hot water from storage tank to the furnace, and the other one for exit the liquid that retains heat from the tank. This liquid such as ethylene glycol or any oily substance that has the property of retaining heat.

Bricks of standard size $(250 \times 120 \times 60)$ mm were used, Egyptian standard, (ASTM C62) "American Society for Testing and Materials", and used sensors to determined center brick temperature.

**Error Analysis of Predicted Results**

A common task in precision agriculture research is to predict the value of a particular variable. For predictions to be correct, the models used must be carefully validated. The goal is to demonstrate that the model produces good estimates of the variable being predicted. For this, at least training and test or validation datasets need to be used. The training dataset is used to create the model, while the test or validation dataset must be used to demonstrate the reliability of the model.

**Root mean square error (RMSE)**

Root Mean Square Error (RMSE) is calculated as follows **(Loague and Green, 1991)**.

$$RMSE = \sqrt{\frac{\sum_{i=1}^{n}(O_i - p_i)^2}{No}} \quad \dots\dots\dots\dots\dots\dots\dots\dots\dots (21)$$

The RMSE represents a measure of the overall, or mean, deviation between observed and predicted values, that is, a synthetic indicator of the absolute model uncertainty. For better model performance the value of RMSE should be near to zero.

**Index of agreement (d)**

The index of agreement (d) was calculated using the **Willmott et al., 1985** equation:

$$d = 1 - \frac{\sum_{i=1}^{n}(O_i - P_i)^2}{\sum_{i=1}^{n}(|P_i - MO| + |O_i - MO|)^2} \quad \dots\dots\dots\dots\dots\dots\dots\dots (22)$$

The Index of Agreement (d) developed as a standardized measure of the degree of model prediction error and varies between $-\infty$ and 1 and the model's fit improves as d approaches unity.

The index of agreement can detect additive and proportional differences in the observed and predicted means and variances; however, it is overly sensitive to extreme values due to the squared differences **(Legates and McCabe, 1999)**.

**Correlation coefficient (r)**

The correlation coefficient (r) is an indicator of degree of closeness between observed values and model predicted value. The observed and predicted values are found to be better correlated as the correlation coefficient approaches to 1. If observed and predicted values are completely independent i.e., they are uncorrelated then r will be zero. The correlation coefficient was estimated by the following equation:

$$r = \frac{\sum_{i=1}^{n}(O_i - MO) \times (P_i - MS)}{\sqrt{\sum_{i=1}^{n}(O_i - MO)^2 \times \sum_{i=1}^{n}(P_i - MS)^2}} \dots\dots\dots\dots\dots\dots\dots\dots\dots\dots\dots (23)$$

% deviation = (predicted – Observed) × 100/ Observed ……………… (24)

## 3. RESULTS AND DISCUSSION

### Predicted the distribution of ground temperatures

The diurnal distributions of ground temperatures were predicted. The amplitudes of wave functions for the diurnal ground temperature at various depths were determined. The ground surface temperature was detected. This temperature was required when applying the energy balance at the furnace false bottom environment. This analysis was carried out to determine the air temperature of the false bottom environment. Moreover, an equation to simulate the diurnal variations of ground temperatures at different depths was also developed. The output results of the numerical model for ground surface temperature and distributions at different depths throughout 24-hours were obtained. They were plotted in Figure (8).

### Predicted brick temperatures

Predicted brick average temperatures were determined using the brick temperature computer model. These temperatures were required to apply the energy analysis on the solar furnace microclimate. The output results of brick average temperatures inside the furnace are plotted in Figure (9). The thermal tank with temperature control and adjusting system was used to fix the brick temperature.

### Brick furnace heating load determination

The output results indicated directly the heating load required inside the solar furnace to dry the unfired brick with a designed interior air temperature at 100 ˚C. Figure (10) demonstrates a computer screenshot of the heating load determination. It had a sine wave pattern. Figure (11) illustrate the effect of ambient air temperature on heating load required in the furnace. As can be seen, the maximum heating load throughout the day was 916.72 Watt. However, the data presented by figure was multiplied by a safety factor 1.2 before it was used in the design of the installed heat exchanger in the furnace. This heat exchanger was used to supply the solar furnace with the required heating load.

### Sizing the installed heat exchanger

The selection of the size and type of the material used for the heat exchanger installed inside the solar furnace were as follows:

- Length of copper tubes was 21 m.
- Inside and outside diameters were 0.9 & 1cm, respectively.
- Number of spiral pipes on each side was 7.
- Pitch between each two spiral pipes was 10 cm.
- Clearance used between the edge of the wall and spiral pipes was 0.004 m.

The solar system components after design were manufactured and installed for field testing. The main thermal components consisted of the unfired brick solar furnace, the installed heat exchanger inside the furnace to provide the heat required for brick curing, vacuum tube, heat exchanger, solar collector, and a thermal storage tank.
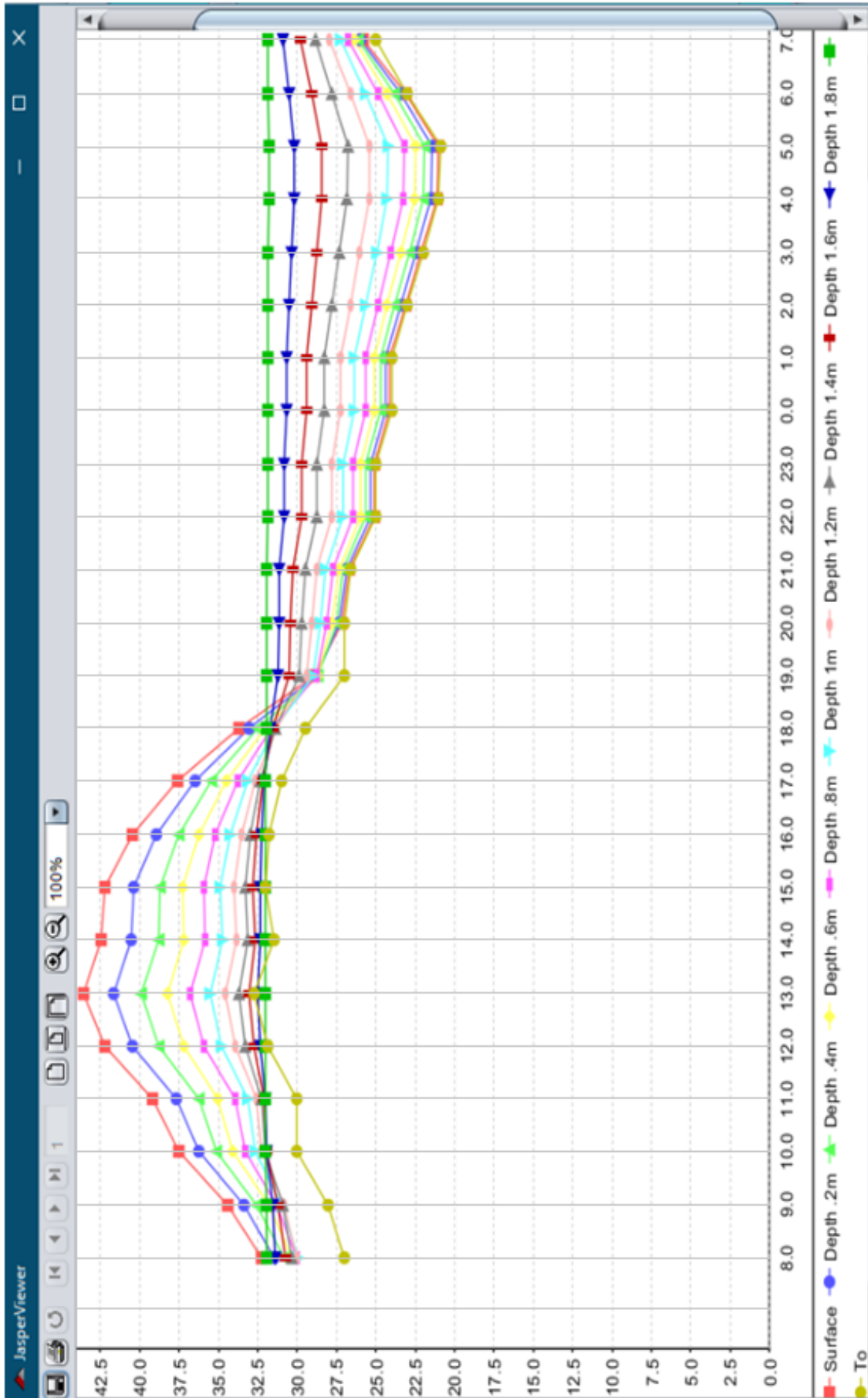
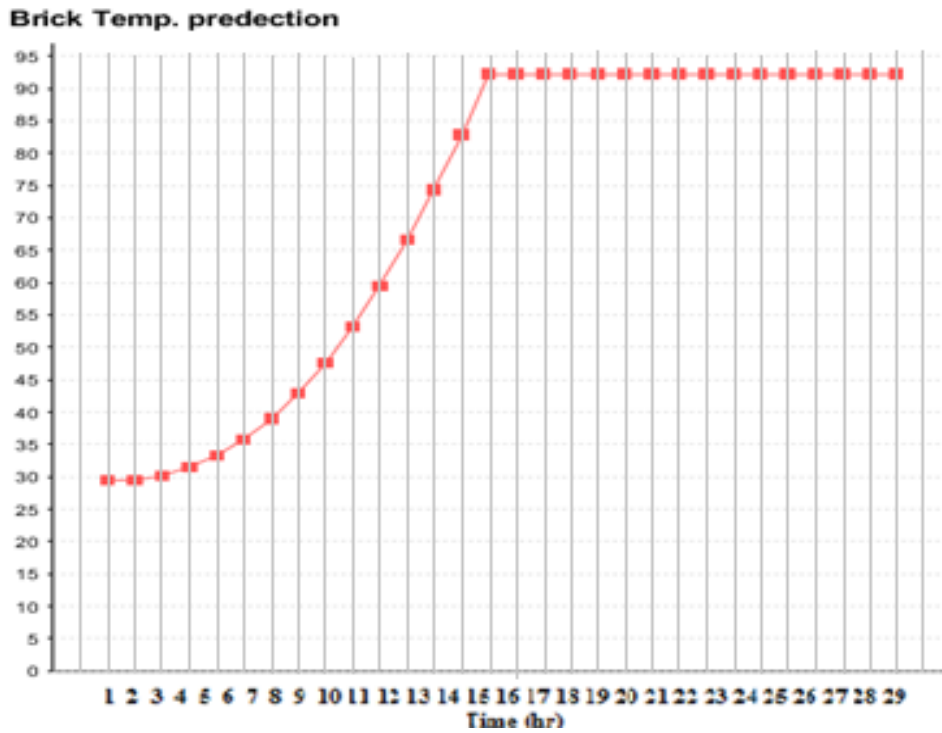**Figure (8): Ground temperature distribution "Sine Wave Function"**
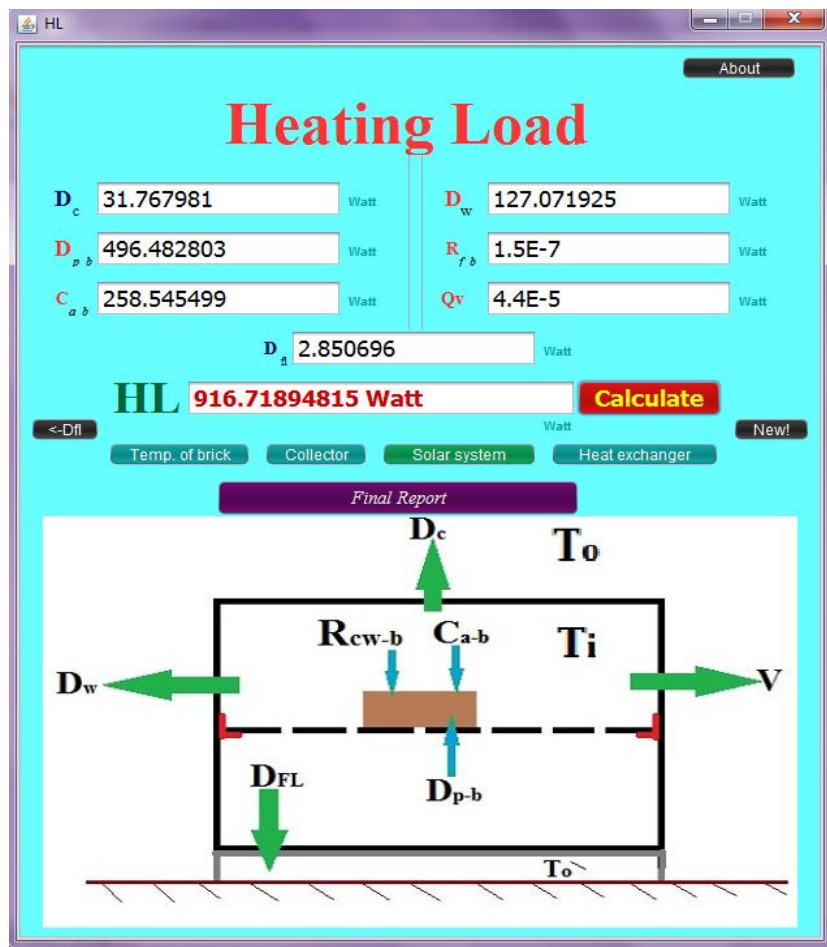
**Figure (9): prediction of brick temperatures**



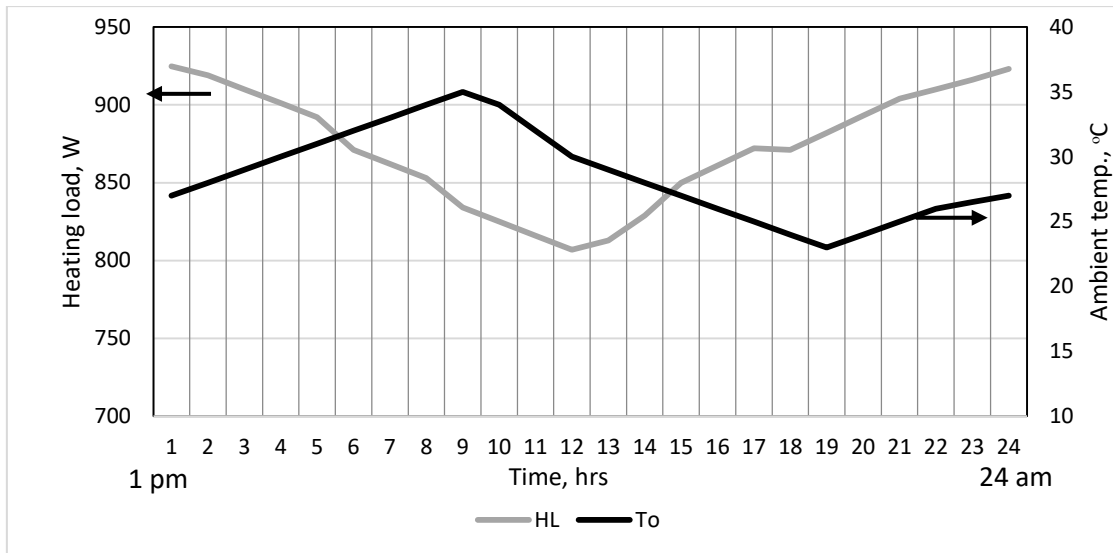**Figure (10): Heating load calculations**

**Figure (11): The pattern of heating load throughout a day**

## Model performance

Figure (12) showed that the final output of the heating load determination and the specific dimensions of the installed heat exchanger (Final report of the output results for all components).

Figure (13) present the measured values of brick temperatures dataset on the abscissa axis and the predicted values on the ordinate axis. Linear regression fits most of the observations.

Note that in the previous equation, the fraction is the ratio of the residual sum of squares to the total data sum of squares. The residuals represent the difference between the prediction and reality. The closer $R^2$ is to 1, the better the prediction, in this figure $R^2 = 0.9823$.

The predicted brick temperature in the solar furnace were compared with the measured values for 25 hours in Table (1), with the deviation of the predicted value from the measured value expressed as a percentage of the measured value and root mean square error (RMSE). Also, index of agreement (d) and the correlation coefficient (r) were presented in the same table for the predicted vs. observed values over the day. It can be seen from Table (1) that when predicted brick temperature is compared with the observed values, with 22 out of the 26 values were within 6% of the measured values, , and 3 out of the 26 deviating more than 6%, with the largest deviation of 15.17%. While the RMSE values were as follows, in total values are low, values were < 0.1 the index of agreement (d) and the correlation coefficient (r) were close to 0.99.

## 4. CONCLUSION

One main program and three subprograms were developed to determine the system design and to describe the performance of a prototype solar furnace. The main program was developed to determine the furnace heating load required to dry unfired bricks. The three subprograms were used developed and with the main program to predict the furnace brick temperature, the furnace ground surface temperature distribution, and the air temperature in the Solar furnace false bottom. The maximum heating load required in the solar furnace was predicted by the simulation model to be 916.73 Watt. This value was used afterwards for sizing the heat exchanger installed inside the furnace to provide the interior recommended air temperature.

## Mathematical model for furance design

| | | |
|---|---|---|
| Area of furance: | 0.25 | M² |
| Inner Temp: | 100.0 | C° |
| **Ambient Temp.** | 28.0 | C° |
| Metal of furance: | steel | |
| Thickness of metal: | copper | |
| Metal of heat exchanger tube: | 31.767981312041865 | |
| Inner diameter of heat exchanger tube: | 9.0E-3 | M |
| Outer diameter of heat exchanger tube: | 0.01 | M |
| Length of heat exchanger tube: | 20.835263 | M |
| No of heat exchanger tube in each side: | 7.0 | |
| Clearence of heat exchanger tube from each edge: | 4.4E-3 | M |
| Dimentions of brick: 0.12 x 0.25 x 0.06 | | M |
| No of brick: | 10.0 | |
| No of pump: 1.0 Power of pump: 48.0 | | W |
| Plenum chamber temp: | 48.690504 | C° |

| | | |
|---|---|---|
| Q D_celing: | 31.767981 | W |
| Q D_plat_brick: | 496.482803 | W |
| Q R(celing-walls): | 1.5E-7 | W |
| Q D_walls: | 127.071925 | W |
| Q C_air-brick: | 258.545499 | W |
| Q ventolation: | 4.4E-5 | W |
| Q D_flor: | 2.850696 | W |
| **Heating Load:** | **916.718948** | W |
| Liqued temp. out of collector: | 107.513155 | C° |
| No of vacume tubes: 9.925194 Length of vacume tubes: 1.8 | | M |
| Diameter of vacume tubes: 0.049 | | M |
| No of panels: 1.0 Panel capacity: 150.0 | | W |
| No of Batteries: 1.0 Battery size: 150.0 | | Am |
| Solar regulator size: 10.0 Am Inverters capacity: 100.0 | | W |

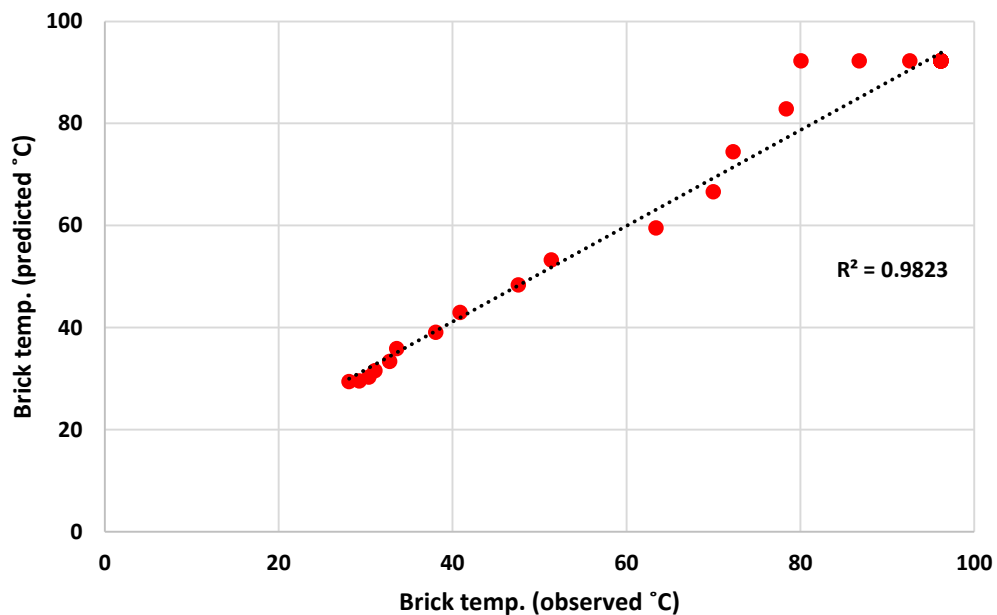**Figure (12): Final report of the output results for all components**



**Figure (13) The relationship between the observed and predicted brick temperature**

Table (1) Predicted compared with observed values and statistical indices derived for evaluating the performance of simulation model in predicted brick temperature.

| Parameters<br><br>Time, hour | Observed °C | predicted °C | Deviation% | RMSE °C | D | R |
|---|---|---|---|---|---|---|
| 0 | 28.1 | 29.4 | 4.62633452 | | | |
| 1 | 29.3 | 29.5 | 0.68259386 | | | |
| 2 | 30.4 | 30.23 | -0.5592105 | | | |
| 3 | 31.1 | 31.48 | 1.22186495 | | | |
| 4 | 32.8 | 33.3 | 1.52439024 | | | |
| 5 | 33.6 | 35.8 | 6.54761905 | | | |
| 6 | 38.1 | 39 | 2.36220472 | | | |
| 7 | 40.9 | 42.9 | 4.88997555 | | | |
| 8 | 47.6 | 48.3 | 1.47058824 | | | |
| 9 | 51.38 | 53.2 | 3.54223433 | | | |
| 10 | 63.41 | 59.5 | -6.1662198 | | | |
| 11 | 70 | 66.6 | -4.8571429 | | | |
| 12 | 72.3 | 74.4 | 2.90456432 | 0.015438 | 0.999 | 0.991 |
| 13 | 78.4 | 82.84 | 5.66326531 | | | |
| 14 | 80.1 | 92.25 | 15.1685393 | | | |
| 15 | 86.8 | 92.25 | 6.27880184 | | | |
| 16 | 92.6 | 92.25 | -0.3779698 | | | |
| 17 | 96.2 | 92.25 | -4.1060291 | | | |
| 18 | 96.2 | 92.25 | -4.1060291 | | | |
| 19 | 96.2 | 92.25 | -4.1060291 | | | |
| 20 | 96.2 | 92.25 | -4.1060291 | | | |
| 21 | 96.2 | 92.25 | -4.1060291 | | | |
| 22 | 96.2 | 92.25 | -4.1060291 | | | |
| 23 | 96.2 | 92.25 | -4.1060291 | | | |
| 24 | 96.2 | 92.25 | -4.1060291 | | | |
| 25 | 96.2 | 92.25 | -4.1060291 | | | |

## 5. REFRENCES

**ASHRAE (2001)**– American Society of Heating, Refrigerating and Air Conditioning Engineers. ASHRAE Handbook – Fundamentals. Atlanta, SI ed.

**Bhat, M. S., Afeefa, Q. S., Ashok, K. P., & Bashir, A. G. (2014)**. Brick kiln emissions and its environmental impact: A Review. *Journal of Ecology and the Natural Environment*, *6*(1), 1-11.

**Chang, C. T., Hong, G. B., & Lin, H. S. (2016)**. Artificial lightweight aggregate from different waste materials. *Environmental Engineering Science*, *33*(4), 283-289.

**Holman, J.P. (1981)** Heat Transfer (International Student Edition). McGraw Hill International Book Co.

**Jamal, J., Tangkemanda, A., & Susanto, T. A. (2018, June)**. The effect of collector slope angle on the performance of solar water heater. In *AIP Conference Proceedings* (Vol. 1977, No. 1, p. 060019). AIP Publishing LLC.

**Kayali, O., Khan, M. S. H., & Ahmed, M. S. (2012)**. The role of hydrotalcite in chloride binding and corrosion protection in concretes with ground granulated blast furnace slag. *Cement and Concrete Composites*, *34*(8), 936-945.

**Legates, D. R., & McCabe Jr, G. J. (1999)**. Evaluating the use of "goodness-of-fit" measures in hydrologic and hydroclimatic model validation. *Water resources research*, *35*(1), 233-241.

**Loague, K., & Green, R. E. (1991)**. Statistical and graphical methods for evaluating solute transport models: overview and application. *Journal of contaminant hydrology*, *7*(1-2), 51-73.

**Shakir, A. A., & Mohammed, A. A. (2013)**. Manufacturing of Bricks in the Past, in the Present and in the Future: A state of the Art Review. *International Journal of Advances in Applied Sciences (IJAAS)*, *2*(3), 145-156.

**Shawabkeh, R. (2015)**. Steps for design of Heat Exchanger. *King Fahd University of Petroleum & Minerals*.

**Sudharsan, N., & Palanisamy, T. (2018)**. A comprehensive study on potential use of waste materials in brick for sustainable development. *Ecology, Environment and Conservation*, *24*(September), S339-S343.

**Turner, L. K., & Collins, F. G. (2013)**. Carbon dioxide equivalent (CO2-e) emissions: A comparison between geopolymer and OPC cement concrete. *Construction and building materials*, *43*, 125-130.

**Willmott, C. J., Ackleson, S. G., Davis, R. E., Feddema, J. J., Klink, K. M., Legates, D. R., & Rowe, C. M. (1985)**. Statistics for the evaluation and comparison of models. *Journal of Geophysical Research: Oceans*, *90*(C5), 8995-9005.

**Nomenclature**

| Symbols | Definition |
|---|---|
| $A_b$ | area of brick, m² |
| $A_c$ | area of ceiling, m² |
| $A_f$ | area of floor, m² |
| $A_p$ | area of performed plate, m² |
| $A_{p-b}$ | Contact area between the perforated plate and the brick, m$^2$ |
| $A_w$ | area of walls, m² |
| $A_{wp}$ | area of plenum walls, m² |
| $C_{g-a}$ | Convection heat exchange between the ground and the furnace bottom, J/s |
| $D_{f-p}$ | Heat transfer from the furnace to the plenum chamber, J/s |
| $D_{Wb}$ | Heat loss through the walls of the plenum chamber, J/s |

| | |
|---|---|
| $T_O^{\prime}$ | The plenum chamber air temperature, (˚C or K) |
| $T_b$ | brick temperature, (˚C or K) |
| $T_g$ | Ground temperature, (˚C or K) |
| $T_o$ | Ambient air temperature, (˚C or K) |
| $V_{inf}$ | Infiltration heat loss from the plenum chamber, J/s |
| $\varepsilon_b$ | emittance factor of the brick |
| $\varepsilon_c$ | emittance factor of the ceiling |
| $\varepsilon_f$ | emittance factor of the floor |
| $\varepsilon_w$ | emittance factor of the walls |
| $\Delta z$ | ground depth, m |
| $\Delta \tau$ | increment of time values, sec |
| 0i | observed value |
| A | area of opening door, m² |
| $C_{a-b}$ | convection heat transfer between the air to the bricks, J/s |
| $Cp_b$ | Brick specific heat, J/kg. C˚ |
| D | The index of agreement |
| $D_c$ | Heat loss from the furnace through the ceiling, J/s |
| $D_f$ | heat loss from the furnace through the floor, J/s |
| $D_{p-b}$ | heat transfer between the performed plate and the brick, , J/s |
| $D_t$ | time of opening door, min /day |
| $D_w$ | heat loss from the furnace through the walls, J/s |
| E | Evaporation heat losses, J/s |
| $F_{(c-b)}$ | The shape factors for the ceiling |
| $F_{(f-b)}$ | The shape factors for the floor |
| $F_{(w-b)}$ | The shape factors for the walls |
| $h_i$ | enthalpy of the air entering the door kj/kg |
| HL | Heating load, J/s |
| $h_r$ | enthalpy of the hot air in the furnace kj/kg |
| I | Incident solar radiation, W/ m$^2$ |
| $m_b$ | Brick mass, kg |
| $M_o$ | mean of observed value |
| MS | mean of predicted value |
| N | number of opening door per day |
| $N_o$ | number of observations |
| Pi | predicted value |
| R | The correlation coefficient |
| $R_{c-b}$ | Radiation from heat exchange between the brick and the ceiling, J/s |
| $R_{f-b}$ | Radiation from heat exchange between the brick and the floor, J/s |
| RMSE | Root mean square error |

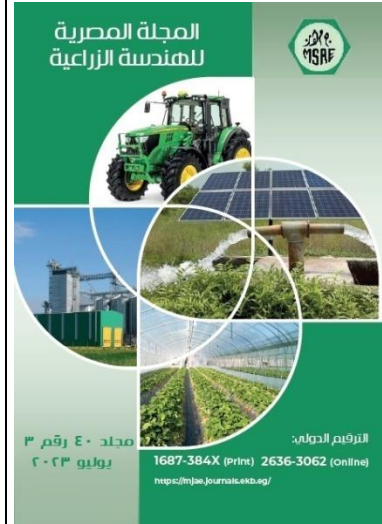| | |
|---|---|
| $R_{w-b}$ | Radiation from heat exchange between the brick and the walls, J/s |
| $T_\infty$ | $T_o$, mean, (˚C or K) |
| Up | The overall coefficient of heat transfer of plate, $Wm^{-2}K^{-1}$ |
| V | ventilation heat loss from opening door of furnace, J/s |
| $\rho_r$ | density of hot air kg/m³ |
| $\Sigma$ | Constant of Stefan – Boltzmann, $5.67 \times 10^{-8}$  W/ m² °K |
| $k$ | Thermal conductivity, W/ m².°K |
| $\gamma$ | Ground absorptivity |
| $\vartheta$ | average velocity of air, m/s |

# نمذجة وتصميم الفرن الشمسي لانتاج طوب الجيوبوليمر

**منى علي محمود¹، محمد حلمى ابراهيم²، محمد ابراهيم نصر³ و احمد عبد العال علي⁴**

¹ طالبة دكتوراة ـ قسم الهندسة الزراعية و النظم الحيوية ـ كلية الزراعة الشاطبي ـ جامعة الإسكندرية ـ مصر.

² أستاذ هندسة النظم البيئة الحيوية والطاقة ـ قسم الهندسة الزراعية و النظم الحيوية ـ كلية الزراعة الشاطبي ـ جامعة الإسكندرية ـ مصر.

³ أستاذ مساعد هندسة النظم البيئة الحيوية والمباني- قسم الهندسة الزراعية و النظم الحيوية ـ كلية الزراعة الشاطبي ـ جامعة الإسكندرية ـ مصر.

⁴ مدرس هندسة نظم الري ـ قسم الهندسة الزراعية و النظم الحيوية ـ كلية الزراعة الشاطبي ـ جامعة الإسكندرية ـ مصر.

## الملخص العربي

أجريت هذه الدراسة بغرض تصميم فرن شمسي يستخدم في تجفيف الطوب ، يتم تسخينه وتشغيله باستخدام الطاقة الشمسية. تم تطوير نموذج رياضي للتنبؤ بتكوين وأداء نظام يتكون من عدة مكونات لإنتاج الطوب الجيوبوليمر. تم تطوير برنامج كمبيوتر باستخدام JavaScript يتكون من برنامج رئيسي وثلاثه برامج فرعية لتصميم النظام الشمسي. وقد استخدمت النتائج المتحصل عليها من برنامج الحاسوب و فروعه الثلاثة في ايجاد نموذج افضل لحجم وتصميم لإبعاد الفرن الشمسي، حجم المبادل الحراري داخل الفرن متضمنا عدد الانابيب والاقطار ، وايضا حجم الخزان الحراري وتم توقع درجة حرارة الطوب. وباستخدام تقنيات تحليل الأخطاء للتحقق من صحة النتائج المتوقعة مقابل القيم المقاسة. كانت النتائج المتوقعة تظهر توافق جيد مع القيم المقاسة ($R^2 = 0.9823$) . وكانت ايضا من النتائج المخرجات المتحصل عليها ان حمل التسخين المطلوب داخل الفرن الشمسي لتجفيف الطوب غير المحروق بدرجة حرارة هواء داخلية مصممة عند ١٠٠ درجة مئوية يتراوح بين أقصى حمل للتدفئة مطلوب "٩١٦,٧٢ وات" عند منتصف الليل وقيمة دنيا "٨١٠ وات" قرب الظهيرة.

وبناء على النتائج المتحصل عليها من البرامج، تم تصميم وتصنيع وتركيب نموذج للفرن الشمسي واستخدامه في الاختبارات.